Climate Dynamics (2021) 56:139–153
https://doi.org/10.1007/s00382-020-05469-y

Quantifying the energetic feedbacks in ENSO

Han Huang[1,2] · Yi Huang[2] · Yongyun Hu[1]

Received: 14 November 2019 / Accepted: 1 October 2020 / Published online: 13 October 2020

Abstract
Energetic feedbacks play important roles during the El Niño-Southern Oscillation (ENSO). Here we conduct a thorough analysis of the radiative and non-radiative vertical fluxes and compare them to horizontal energy transport to provide a complete view of the energetics of ENSO. Our analyses affirm that cloud feedbacks are the most important radiative feedbacks, with cloud shortwave (SW) and longwave (LW) feedbacks dominating at the surface and in the atmosphere respectively. Oceanic energy transport dominates the oceanic heat content change in the developing phase and has significant effects on the sea surface temperature (SST) about 6 months earlier than vertical fluxes. Atmospheric horizontal energy transport is also important, acting to quickly remove the surplus of energy provided by the convergence of vertical energy fluxes in the atmosphere. The differential diabatic heating between the Central Pacific and the Warm Pool, induced by the latent heat release as well as LW radiation, strengthens the anomalous circulation and reinforces the Bjerknes positive feedback to strengthen the SST anomaly. This work reveals that the differential heating is more strongly correlated with the SST anomaly in the Central Pacific than the local SW negative feedback of clouds and supports the idea that the overall atmospheric effect is likely a positive feedback that acts to strengthen ENSO.

Keywords Climate feedback · Energy budget · ENSO

1 Introduction

The El Niño-Southern Oscillation (ENSO) is the dominant mode of interannual variability in the tropical climate system. The predominant characteristic of ENSO is associated with the SST anomalies in the Tropical Pacific which are accompanied by the movement of convective activities and together have the ability to significantly impact local climate and even climate variability in remote regions (Klein et al. 1999; Chiang and Sobel 2002; Trenberth et al. 2002; Liu and Alexander 2007). The transition between the ENSO warm phase (El Niño) and cold phase (La Niña) is also coupled with the weakening or strengthening of atmospheric circulations, such as the Walker circulation (Bjerknes 1966; Bayr et al. 2014). During the El Niño phase there are more convective activities in the Central Pacific which are accompanied by an increase of convective clouds and precipitation. With more clouds reflecting incoming solar radiation and more latent heat released by precipitation, the ENSO events also have a great impact on the local energy budget (Trenberth and Stepaniak 2003; Sun et al. 2006; Roemmich and Gilson 2011; Mayer et al. 2013; Pinker et al. 2017), which can further impact the amplitude of ENSO. Therefore, it is important to quantify the effects of energetic processes in such a highly coupled system.

Previous studies have investigated radiative and non-radiative feedbacks during ENSO events. Many studies have noted that shortwave (SW) (Waliser et al. 1994; Sun and Trenberth 1998; Cess et al. 2001; Guilyardi et al. 2009) as well as latent heat feedbacks (Lloyd et al. 2009) are the primary negative feedbacks during the ENSO in both the model simulations and observations. Lloyd et al. (2009) noticed that the strength of the atmospheric net heat fluxes (the sum of SW, LW, latent and sensible heat) over the Niño 3 region is inversely related to the ENSO amplitude in the Coupled Model Intercomparison Project

Electronic supplementary material The online version of this article (https://doi.org/10.1007/s00382-020-05469-y) contains supplementary material, which is available to authorized users.

✉ Han Huang
han.huang1327@gmail.com

[1] Department of Atmospheric and Oceanic Sciences, School of Physics, Peking University, Beijing, China

[2] Department of Atmospheric and Oceanic Sciences, McGill University, Montreal, QC, Canada

phase 3 (CMIP3) models. Among all the radiative feedbacks during the ENSO, previous works were mostly concerned with the feedbacks induced by changes in water vapor, temperature, and clouds (Zhang and Sun 2008; Sun et al. 2009; Dessler 2013). For example, some researchers have demonstrated a stronger positive water vapor feedback and weaker cloud SW feedback in the models than in the observations (Sun et al. 2003, 2006, 2009; Guilyardi et al. 2009; Dessler 2013) and that the cloud feedback has the greatest uncertainty either from the comparison among the models or between the model simulations and the observations (Lloyd et al. 2012; Dessler 2013; Bellenger et al. 2014; Wang and Su 2015). Apart from acting as a radiative feedback, cloud changes are closely related to large-scale atmospheric circulation changes in both the observations and model simulations (Allan et al. 2002; Su and Jiang 2013; Rädel et al. 2016). Together the cloud radiative effects and changes to the atmospheric circulation can approximately double the amount of ENSO variability by enhancing the Bjerknes feedback (Rädel et al. 2016). Therefore, cloud changes can lead to either a positive feedback of SST warming via the Bjerknes feedback or a negative feedback by reflecting more SW radiation to the space. In short, it is still debated whether the atmospheric overall feedback enhances or dampens SST variability.

To gain a better understanding of the role of each radiative feedback, Kolly and Huang (2018) used a reanalysis-based kernel dataset to investigate the radiative feedbacks over the entire tropical region and quantified the radiative feedbacks at the TOA and the surface as well as in the atmosphere. Not included in their study, however, are the non-radiative energy flux feedbacks which also have a great impact on the ENSO evolution. Previous research has indicated that the atmospheric model used in the study plays a dominant role in modeling ENSO in GCMs (Guilyardi et al. 2004; Sun et al. 2009; Lloyd et al. 2011), through the interaction of dynamical, radiative (SW + LW), and non-radiative (sensible and latent heat) feedbacks. In addition to these feedbacks, the horizontal energy transport both in the atmosphere and ocean are also of great importance. Sun (2000) investigated the 1986/87 El Niño and suggested that the cloud negative feedbacks caused by the increase of SW radiation reflected by clouds is small compared to the enhanced poleward energy transport negative feedbacks in the atmosphere and ocean. Some studies showed that underestimating the strength of the net atmospheric feedback (including both cloud SW and atmospheric transport negative feedbacks) in the models contributes to a weaker dampening effect on the SST than in the real world (Sun et al. 2003, 2006). Therefore, it is necessary to include non-radiative fluxes as well as horizontal energy transport in a comprehensive analysis. In this paper, we include both radiative and non-radiative flux feedbacks, in comparison with horizontal energy transport feedbacks, to give a complete picture of how different feedbacks work in relation to each other in ENSO.

While cloud feedbacks are of great significance during the ENSO evolution there remains the issue of the uncertainty of its quantification (Bony and Dufresne 2005; Stephens 2005) which is related to either the method of computing the cloud feedback or the data itself. Previous studies have used cloud radiative forcing (CRF) or the kernel method to quantify cloud radiative feedbacks (Soden et al. 2004; Shell et al. 2008; Dessler 2010; Radley et al. 2014; Middlemas et al. 2019). The results presented by these works can vary significantly. Sun and Trenberth (1998) used the Earth Radiation Budget Experiment (ERBE) dataset and the CRF method to measure cloud feedbacks at the TOA over the entire Tropical Pacific during the 1986/87 ENSO event and indicated a SW CRF of about − 6.2 W/(m^2 K) and a LW CRF of approximately 8.1 W/(m^2 K). Later, Sun et al. (2006) who used the ERBE and the European Centre for Medium-Range Weather Forecast reanalysis (ERA40) dataset determined that the SW and LW cloud feedbacks over the Equatorial Pacific were − 10.93 W/(m^2 K) 12.21 W/(m^2 K), respectively. Dessler (2013), on the other hand, used the kernel method and both the ERA-Interim (ERAI) and the Modern-Era Retrospective Analysis for Research and Applications (MERRA) datasets to measure the average global cloud feedback for the 2000–2010 period. Although the difference between the net cloud feedback of the two datasets was consistently measured to be approximately 0.5 W/(m^2 K), the LW and SW components were noticeably different in these two datasets. Therefore, it is necessary to make a thorough comparison of the cloud feedback among different methods and datasets. Here we analyze the cloud feedbacks analyzed using both the CRF and kernel methods, based on different datasets, to investigate the uncertainty induced by these factors.

The discussions above show that it is important to investigate the relationship between the SST evolution and radiative as well as non-radiative feedbacks, especially to ascertain the role of atmospheric feedbacks—whether they enhance or dampen the SST warming. Furthermore, as the cloud feedback is of great importance, it is necessary to measure the uncertainty in its quantification. In this paper, we mainly use the kernel method to derive radiative feedbacks and analyze the non-radiative flux, especially the horizontal energy flux feedback, to show a complete picture of the relationship between all feedbacks and SST evolution during ENSO events. In addition, we make a comparison of cloud feedback analyzed from different methods and datasets to measure its uncertainty. The structure of this paper is as follows: Sect. 2 describes the methods and datasets, Sect. 3 discusses the relationship between all feedbacks and SST warming, and Sect. 4 summarizes the results.

2 Methodology

2.1 Energy budget equations

The energy budget equations in the atmosphere and ocean can be expressed using Eqs. (1) and (2) (Mayer et al. 2017; Cheng et al. 2019).

$$\left(\frac{\partial E}{\partial t}\right)_{atm} = R_{net\_toa} - \left(R_{net_{sfc}} + LH + SH\right) + \nabla \cdot F_{atm} + res \tag{1}$$

$$\left(\frac{\partial E}{\partial t}\right)_{ocn} = R_{net\_sfc} + LH + SH + \nabla \cdot F_{ocn} \tag{2}$$

Here in Eq. (1), $E = \frac{1}{g}\int_0^{p_s}\left(c_pT + Lq + \Phi_s + k\right)dp$, is the vertical integrated total energy in the atmosphere, p_s is the surface pressure, q is the specific humidity, c_p is the specific heat of air at constant pressure, T is the air temperature with units of Kelvin, L is the latent heat of vaporization, Φ_s is the surface geopotential, k is the kinetic energy, and dp is the pressure difference. The $\left(\frac{\partial E}{\partial t}\right)_{atm}$ term represents the energy tendency in the atmosphere and is determined by taking the difference of the daily mean total energy in the atmosphere between the last day and the first day in one month. Because of the small heat capacity in the atmosphere, the monthly variation of $\left(\frac{\partial E}{\partial t}\right)_{atm}$ is negligible (Fig. 1). R_{net_toa} and R_{net_sfc} are the net radiative fluxes at the TOA and the surface, respectively. LH is the latent heat induced by evaporation and SH is the sensible heat at the surface. $\nabla \cdot F_{atm}$ is the horizontal energy transport in the atmosphere while res is the residual term as there remains a non-closure even based on the energy fluxes provided by the reanalysis dataset itself. We list the non-closures of each dataset in Table S1. In

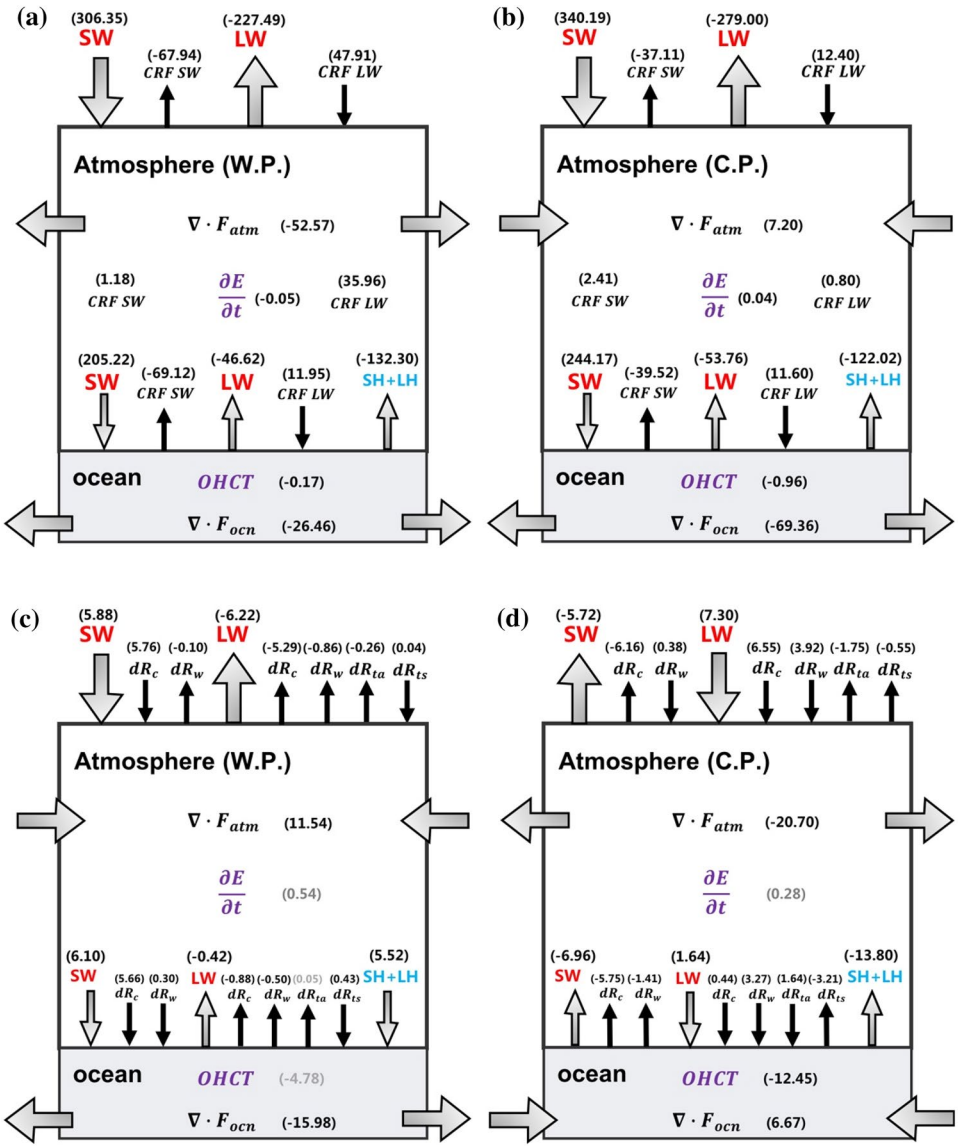

Fig. 1 Schematic of an energy budget based on ERA5 data in the **a**, **c** Warm Pool (W.P., 5N–5S, 120E–150E) and **b**, **d** Central Pacific region (C.P., 5N–5S, 190E–240E), with **a**, **b** climatology, units: W/m^2, and **c**, **d** feedbacks, units: W/(m^2 K). Grey numbers indicate insignificant results (insignificant correlation between SST anomaly and energy flux anomaly)

Eq. (2) $\left(\frac{\partial E}{\partial t}\right)_{ocn}$ is the ocean heat content tendency term (OHCT) and $\nabla \cdot F_{ocn}$ is the oceanic energy flux transport. All vertical fluxes are defined downward positive. A positive convergence of horizontal energy flux in the atmosphere or in the ocean indicates a warming effect.

To obtain all the energy fluxes above and measure their spread among various datasets, we mainly use three reanalysis datasets: the fifth generation of European Centre for Medium-Range Weather Forecasts (ERA5) atmospheric reanalysis (Hersbach et al. 2020), ERA-Interim (Dee et al. 2011), and Japanese 55-year Reanalysis (Kobayashi et al. 2015). Satellite observations are also included to compare radiative fluxes with reanalysis datasets.

2.2 Radiative fluxes

For all-sky vertical radiative fluxes (R_{net_toa} and R_{net_sfc}), we compare the results from the three reanalysis datasets to the monthly averaged dataset obtained using the Energy Balanced and Filled (EBAF) Ed4.0 product from Clouds and the Earth's Radiant Energy System (CERES) (Loeb et al. 2018), which is based on direct satellite observations. We find that the results from ERA5 are in the best agreement with those from the CERES. Since clear-sky radiative fluxes from the CERES are subject to errors in the radiative transfer model, as are reanalysis datasets, to keep consistency with the data source of horizontal energy transport in the atmosphere, clear-sky radiative fluxes are taken from reanalysis datasets. To assess the uncertainty of clear-sky radiative fluxes, we also use the CERES EBAF Ed4.1 product, which defines clear-sky in the same way as general climate models (GCMs), allowing us to make a comparison of the results from the combination of CERES EBAF Ed 4.0 and reanalysis datasets., Note that the combination of the all-sky radiative flux from CERES and clear-sky radiative flux from ERA5 will be denoted as CERES-ERA5 throughout this paper, while all-sky and clear-sky radiative fluxes both from reanalysis dataset will be denoted as ERA5, ERAI and JRA55.

2.2.1 Radiative kernels

To decompose the total radiative flux change into different components, we use the kernel method to attribute the total radiation anomalies to the contributions from water vapor (wv), air temperature (ta), surface temperature (ts) and clouds (c):

$$dR = dR_{ta} + dR_{ts} + dR_{wv} + dR_{c} \tag{3}$$

Here dR represents the total radiative anomalies at the TOA or surface. The non-cloud components dR_x are computed as:

$$dR_x = \frac{\partial R}{\partial x} \times \Delta x \tag{4}$$

We define $K_x = \frac{\partial R}{\partial x}$ as the radiative sensitivity kernels of the non-cloud components (ta, ts, wv), which are pre-calculated by a radiative transfer model (Huang et al. 2017). $\Delta \boldsymbol{x}$ is the anomaly of the non-cloud variable $\boldsymbol{x}$ (ta, ts, wv) and is measured as the deviation from its climatological value. Figure S1 in the Supplementary Information shows a good radiation closure, the kernel-diagnosed radiation change well reproducing the clear-sky radiation change in the dataset. This verifies the consistency between the atmospheric variables and radiation anomalies used in this analysis. The cloud radiative effect, dR_c, is quantified by the adjusted cloud radiative forcing method (Shell et al. 2008):

$$\begin{aligned} dR_c &= \Delta R - \Delta R^o + \sum dR_x^o - \sum dR_x \\ &= dCRF + \sum dR_x^o - \sum dR_x \end{aligned} \tag{5}$$

where the superscript ^{o} indicates components of clear-sky and $\sum dR_x$ represents the sum of all non-cloud components. dR_c measured in this way includes the nonlinear effects associated with the residual terms, although the magnitudes of these terms are small (Figure S1). $dCRF$ represents the change in cloud radiative forcing, measured by the difference of the radiative flux between all-sky and clear-sky conditions: $dCRF = \Delta(R - R^o)$. Each radiative anomaly can be partitioned into LW and SW components. Radiative anomalies in the atmosphere are the differences between those at the TOA and the surface:

$$dR^{atm} = dR^{toa} - dR^{sfc} \tag{6}$$

For example, the water vapor radiative effect in the atmosphere can be obtained by $dR_{wv}^{atm} = dR_{wv}^{toa} - dR_{wv}^{sfc}$.

2.3 Non-radiative fluxes

In this paper, the heat flux ($LH + SH$) at the surface, the horizontal energy transport in the atmosphere and the oceanic energy transport are all denoted as non-radiative fluxes.

2.3.1 Horizontal energy transport in the atmosphere

To calculate the horizontal energy transport in the atmosphere, we use the four-times daily analysis of state variables of model resolution from reanalysis datasets (JRA55, TL319 and 60 vertical hybrid model levels; ERAI, TL255 and 60 vertical hybrid model levels; ERA5, TL639 and 137 vertical hybrid model levels). However, mass flux corrections are needed to make the results meaningful (Figure S2) and the convergence of total energy in the atmosphere should be calculated as in Eq. (7) (Mayer et al. 2017)

$$\nabla \cdot F_{atm} = -\nabla \cdot \frac{1}{g} \int_0^{p_s} [(1-q) \times c_p \times (T - T_{00}) + \Phi + Lq + k] V dp \tag{7}$$

Here, $\nabla \cdot F_{atm}$ is the horizontal energy transport in the atmosphere [the same as in Eq. (1)], T_{00} is 273.16 K, Φ is the geopotential, and $\boldsymbol{V}$ is the 2D horizontal wind vector. All other variables are the same as in the definition of E in Eq. (1). Note that the horizontal energy flux fields in the atmosphere are smoothed by a triangular truncation with a maximum wavenumber of 255 and the Hoskins-type spectral filter: $S_n = e^{-\left(\frac{n(n+1)}{n_0(n_0+1)}\right)^2}$, with n being the wavenumber (from 0 to 255) and $n_0 = 45$ (Sardeshmukh and Hoskins 1984).

2.3.2 Heat flux at the surface (*LH* + *SH*)

Since the observations of energy flux at the surface are rare and the estimation of the non-radiative fluxes (e.g. *LH* and *SH*) exhibits large uncertainties, we compare the heat flux at the surface directly from reanalysis datasets and the heat flux inferred from the radiative flux and the horizontal energy transport in the atmosphere. The inferred heat flux at the surface is obtained using Eq. (8),

$$heat\,flux = LH + SH = R_{net\_toa} - R_{net\_sfc} + \nabla \cdot F_{atm} \tag{8}$$

where R_{net_toa} and R_{net_sfc} are net radiative flux at the TOA and the surface from the CERES or reanalysis data (see Table S1) and $\nabla \cdot F_{atm}$ is the horizontal energy transport in the atmosphere from the reanalysis datasets. See Tables S1 and S2 and Figure S3 for comparisons of the heat flux from this method and those obtained directly from the reanalysis products. For example we find that the climatological heat flux ($LH + SH$) inferred from Eq. (9) (Table S1 in the Supplementary Information) is slightly weaker in the Central Pacific than the direct reanalysis output (except for ERAI) but slightly stronger in the Warm Pool region. The heat flux directly from the JRA55 output is stronger than those from the other datasets. Despite these discrepancies, the conclusion that the heat flux is a strong energy sink at the surface in climatology is not sensitive to which dataset is used. Table S2 compares the heat flux feedbacks across datasets and confirms that the surface heat flux feedback is a strong negative feedback to the local SST changes during the ENSO. Because the radiative fluxes from ERA5 show best agreement with the CERES observations and the residual pattern from ERA5 is less biased than the other two datasets, we present our analyses (the figures and tables in the Results section) mainly using the results (including radiative fluxes, horizontal energy transport in the atmosphere and derived surface heat fluxes) based on ERA5, and the results from other datasets are provided in the Supplementary Information for comparison.

2.3.3 Non-radiative fluxes in the ocean

The $\left(\frac{\partial E}{\partial t}\right)_{ocn}$ ($OHCT$) term from Eq. (2) is obtained from Cheng et al. (2017), which is an ocean analysis dataset for the upper 2000 m from the Institute of Atmospheric Physics based on ocean subsurface temperature observations from various instruments, and smoothed by the method in Cheng et al. (2019). The oceanic energy flux transport ($\nabla \cdot F_{ocn}$) is determined as a residual and represents the effects of both horizontal and vertical transports.

$$\nabla \cdot F_{ocn} = \left(\frac{\partial E}{\partial t}\right)_{ocn} - R_{net\_sfc} - (LH + SH) \tag{9}$$

2.3.4 Differential heating in the atmosphere

In this paper, we are also interested in how differential heating in the atmosphere contributes to the anomalous atmospheric circulation and how this impacts the evolution of SST. As the SW radiative anomalies in the atmosphere are small during the ENSO (Fig. 4a), we are only concerned with LW anomalies and latent energy released by condensation (LC) in the atmosphere as the predominant sources of differential heating (note that here latent heat release by condensation is determined differently from LH in Eqs. (1) and (2), which is derived from surface evaporation). Precipitation data is taken from the Tropical Rainfall Measuring Mission (TRMM), which provides a good estimate of precipitation from 50 N to 50S (Huffman et al. 2010). Differential heating is defined as the difference of anomalous energy flux between the Central Pacific (5N–5S, 190–240E) and the Warm Pool (5N–5S, 120–150E) region, with positive values indicating more atmospheric heating in the Central Pacific than in the Warm Pool. The same analysis with precipitation from ERA5 is also conducted (not shown) and the results are consistent with those based on the TRMM data.

2.4 Feedback quantification

In this paper, we use a regression between flux anomalies and Oceanic Niño Index (ONI) to measure feedback strength and refer to the regression coefficients as feedbacks.

$$flux_{ano} = \lambda_X \times ONI + b \tag{10}$$

Here ONI is the monthly SST anomalies measured over the Nino 3.4 region (5N–5S, 190–240E, the same as the Central Pacific) and $flux_{ano}$ is the anomalous flux relative to the January 2001 to December 2016 climatological mean. Note that $flux_{ano}$ can be either a radiative or non-radiative flux. For the radiative flux, $flux_{ano}$ represents either the total radiative anomalies or the radiative anomalies quantified

from the kernel method, such as dR_{ta}, dR_{ts}, dR_{wv} and dR_c. In this paper, the regression coefficient λ_X is defined as the feedback [units: W/(m^2 K)] and b is the intercept from the regression. We apply a lagged regression method to investigate the evolution of vertical and horizontal energy fluxes during the different phases of ENSO. A correlation analysis is also used to identify the component feedbacks that are the most associated with the SST change. A "*significant*" correlation means results passing the 95% confidence level test if not otherwise noted. Note that the feedback results from the regression analysis are shown only when they are significant at the 95% confidence level (e.g. in Figs. 2, 3, 4).

3 Results and discussions

3.1 Energy budget

Figure 1 shows a schematic of the climatological and anomalous energy budgets of the atmosphere–ocean system over the Central Pacific and Warm Pool region. Results from other datasets or combinations are shown in Table S1 and S2, which are consistent with the results used here (ERA5). In the climatology (Fig. 1a, b), the negative *CRFSW* exceeds *CRFLW*, indicating that clouds in both two regions have a cooling effect on the local climate. In the Warm Pool region, the cloud radiative effect is much stronger than that in the Central Pacific because of the existence of more convective clouds in the Warm Pool region. The convective clouds also help to heat the atmosphere in the Warm Pool region more so than in the Central Pacific (comparison of *CRFLW* in the atmosphere between these two regions), which enhances the

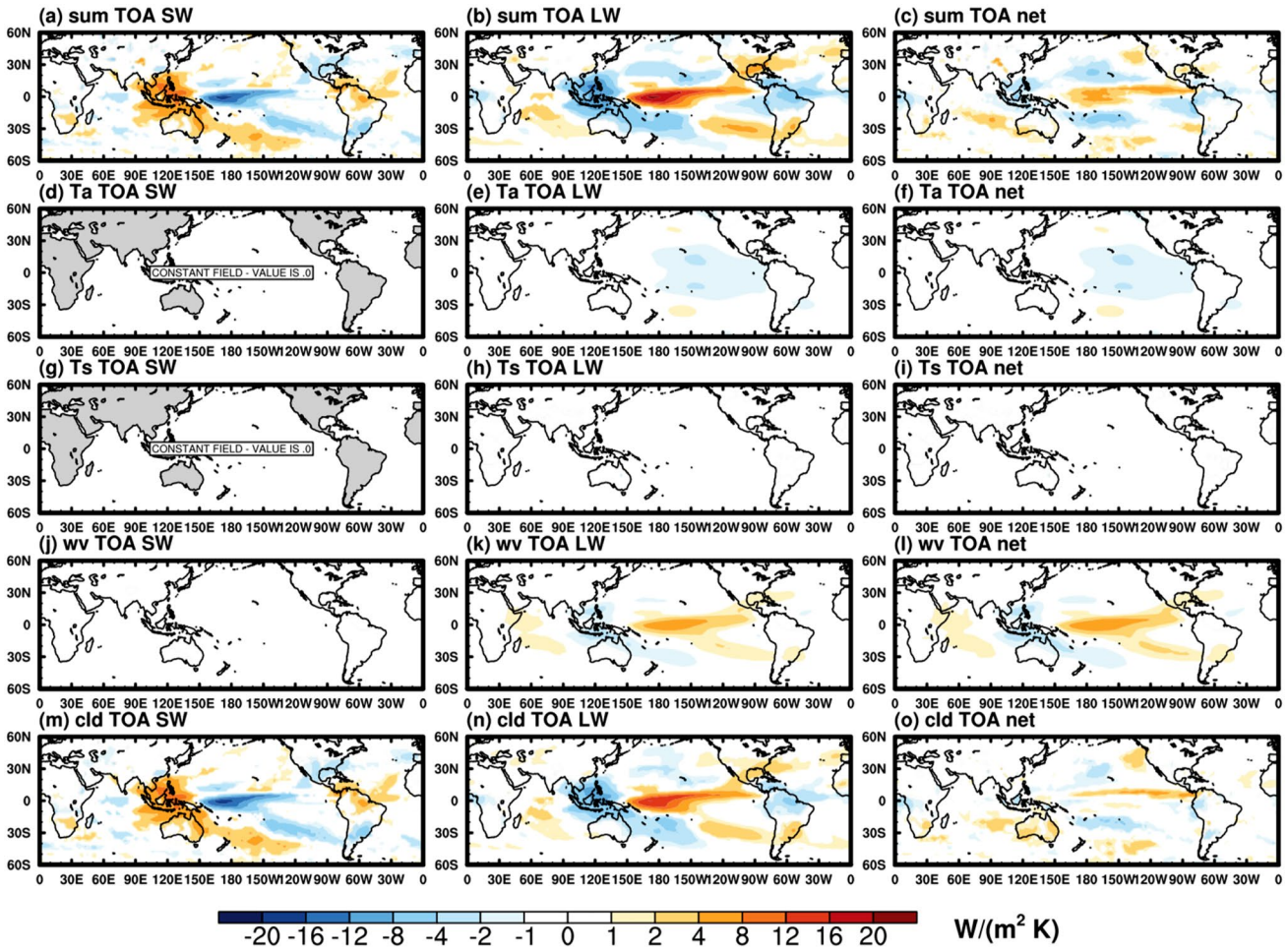

Fig. 2 Radiative feedbacks at the TOA, units: W/(m^2 K). **a**, **d**, **g**, **j**, **m** SW feedbacks. **b**, **e**, **h**, **k**, **n** LW feedbacks. **c**, **f**, **i**, **l**, **o** net radiative feedbacks, SW + LW. *sum* denotes the total radiative feedback; T_a, the air temperature feedback; T_s is the surface temperature feedback; *wv*, the water vapor feedback; *cld*, the cloud feedback. Note that only values passing the 95% significance test are contoured in color

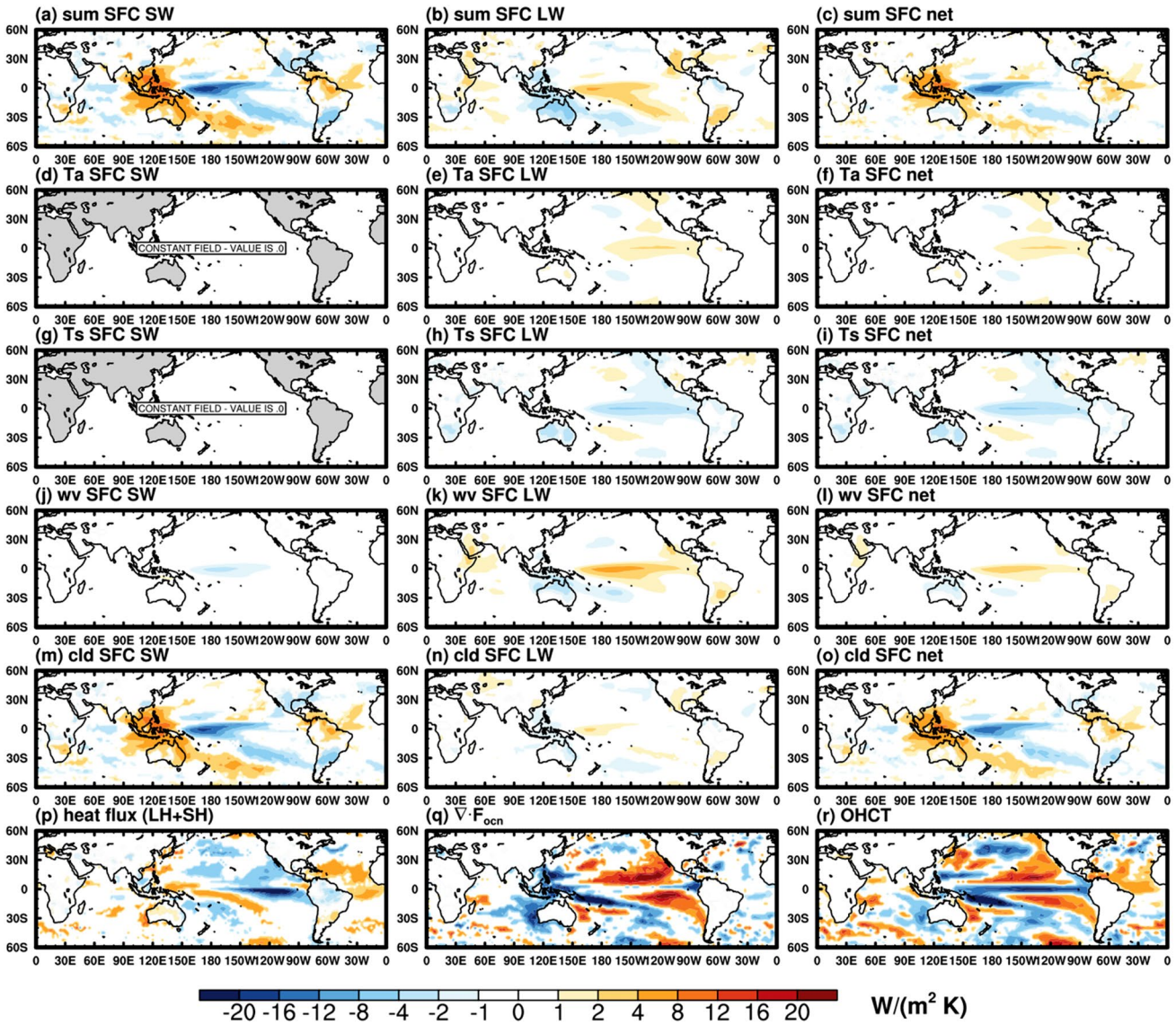

Fig. 3 Radiative and non-radiative feedbacks at the surface, units: W/(m^2 K). **a**, **d**, **g**, **j**, **m** SW feedbacks. **b**, **e**, **h**, **k**, **n** LW feedbacks. **c**, **f**, **i**, **l**, **o** net radiative feedbacks, SW + LW. *sum* denotes the total radiative feedback; T_a the air temperature feedback; T_s is the surface temperature feedback; *wv*, the water vapor feedback; cld, the cloud feedback. (p) heat flux feedback. (q) oceanic energy transport feedback. (r) ocean heat content tendency. Note that only values passing the 95% significance test are contoured in color

ascending motion of air in that region. Strong ascending motion in the atmosphere over the Warm Pool corresponds to the strong divergence of horizontal energy flux in the atmosphere. While in the Central Pacific, the descending branch of the Walker Circulation corresponds to the convergence of the horizontal energy flux in the atmosphere. The heat fluxes at the surface are similar in these two regions and there is a strong divergence of the oceanic energy transport in both of these regions.

Because of the opposite SST anomalies and the movement of convective systems, the changes of the energy budget in the Warm Pool region and Central Pacific during ENSO are opposite to each other. The increase of cloud cover induced by the anomalously warm SST in the Central Pacific results in more reflectance of SW and thus a negative SW feedback at the TOA. Furthermore, the enhancement of convective activities and the associated ascending motion in the atmosphere leads to more divergence of horizontal atmospheric energy flux in that region. Since the SST anomaly in the Warm Pool region is opposite to that in the Central pacific, the change of the energy flux differs from that in the Central Pacific, with more SW reaching the surface and more convergence of horizontal energy transport in the atmosphere. In general, the strengths of SW feedback and LW feedback at the TOA are comparable but of the opposite signs, although the strength of these feedbacks exhibits

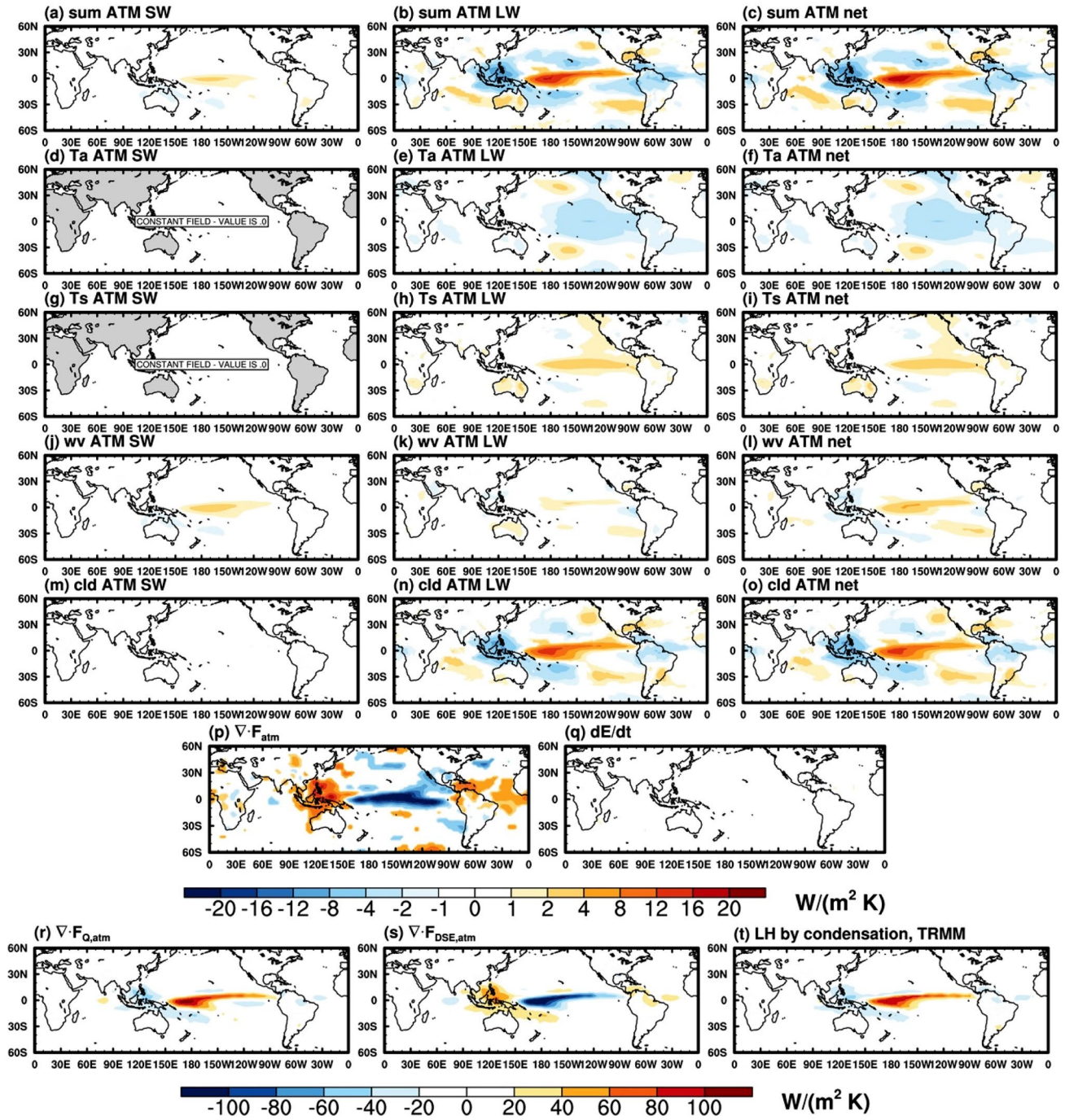

Fig. 4 Radiative and non-radiative feedbacks in the atmosphere, units: W/(m^2 K). **a**, **d**, **g**, **j**, **m** SW feedbacks. **b**, **e**, **h**, **k**, **n** LW feedbacks. **c**, **f**, **i**, **l**, **o** net radiative feedbacks, SW + LW. *sum* denotes the total radiative feedback; T_a the air temperature feedback; T_S is the surface temperature feedback; *wv*, the water vapor feedback. *cld*, the cloud feedback. (p) horizontal energy transport feedback in the atmosphere. (q) energy tendency feedback in the atmosphere. (r) horizontal transport of latent heat in the atmosphere. (s) horizontal transport of dry static energy. (t) latent heat release by condensation. Note that the horizontal energy flux feedbacks in the atmosphere (p, r, s) are smoothed by a triangular truncation and a Hoskins-type spectral filter. Only values passing the 95% significance test are contoured in color

slight variability among the different datasets. Next we will analyze the change of each energy component during ENSO, with respect to the different budgets.

3.1.1 TOA

The LW and SW feedbacks at the TOA compensate each other well, leading to a small net feedback to the local climate system. Both the LW and SW feedbacks are primarily induced by cloud property changes (Fig. 2) because of the movement of convective activity, with the SW cloud radiative effect dominated by cloud cover change and LW cloud radiative effect contributed by both the change of cloud cover and cloud top pressure (Wang and Su 2015). It is interesting to note that the temperature warming-resulted TOA LW feedback arises mainly from the atmospheric warming rather than the surface warming. Although SST in the Central Pacific can increase by several Kelvins during El Niño, which emits more radiative energy (a negative feedback), the high water vapor concentrations in the atmosphere can absorb most of the increased surface emission, which leads to very little increase in the outgoing LW radiation flux at the TOA (Fig. 2h). On the other hand, the warm SST anomaly in the Central Pacific is accompanied by atmospheric warming and the enhanced LW emission from the atmosphere leads to noticeably more outgoing LW radiation (a negative feedback) at the TOA (Fig. 2e). As the change of temperature has no effect on SW, Fig. 2d, g has a uniform zero value field. As a warm SST anomaly develops in the Central Pacific, the water vapor concentration in the atmosphere also increases and enhances the water vapor greenhouse effect, resulting in a positive water vapor LW feedback. Meanwhile, a decrease of water vapor in the Warm Pool region leads to a negative water vapor LW feedback (Fig. 2k).

3.1.2 Surface

Figure 3 shows both radiative and nonradiative feedbacks at the surface. Among all radiative feedbacks, the cloud SW feedback dominates over the Tropical Pacific. With more clouds in the Central Pacific, the cloud feedback reduces the SW radiation at the surface and acts as a negative feedback to the local surface warming (Fig. 3m). Interestingly, the increase of cloud cover in the Central Pacific does not lead to a significant increase of downward LW radiation at the surface (Fig. 3n). This is because the high concentration of water vapor in the boundary layer makes the LW radiation insensitive to the changes in clouds. As mentioned before, the warming of SST in the Central Pacific enhances LW emissions upwards from the surface and is a strong negative LW feedback (Fig. 3h). SST warming in the Central Pacific warms the near-surface atmosphere and leads to enhanced downward LW emissions from the lower atmosphere to the surface, which is a positive LW feedback to the surface warming (Fig. 3e). The increase of water vapor concentration enhances the opacity of the atmosphere, trapping more LW in the atmosphere which results in more LW radiation directed towards the surface (Fig. 3k).

Non-radiative feedbacks, such as the heat flux and oceanic energy transport feedbacks, also have opposite signs between the West and Central/East Pacific during El Niño. In the Central/East Pacific, positive SST anomalies induce a higher temperature gradient between the sea surface and near surface air and thus leads to more *SH* into the atmosphere; the positive SST anomalies also cause more evaporation, and more *LH* (Fig. 3p). The oceanic energy transport feedback in the Central Pacific region is of small magnitude when synchronized with SST warming (Fig. 5, at zero-lag). However, ocean dynamics start to take effect about 12 months before significant SST warming occurs and contribute most during

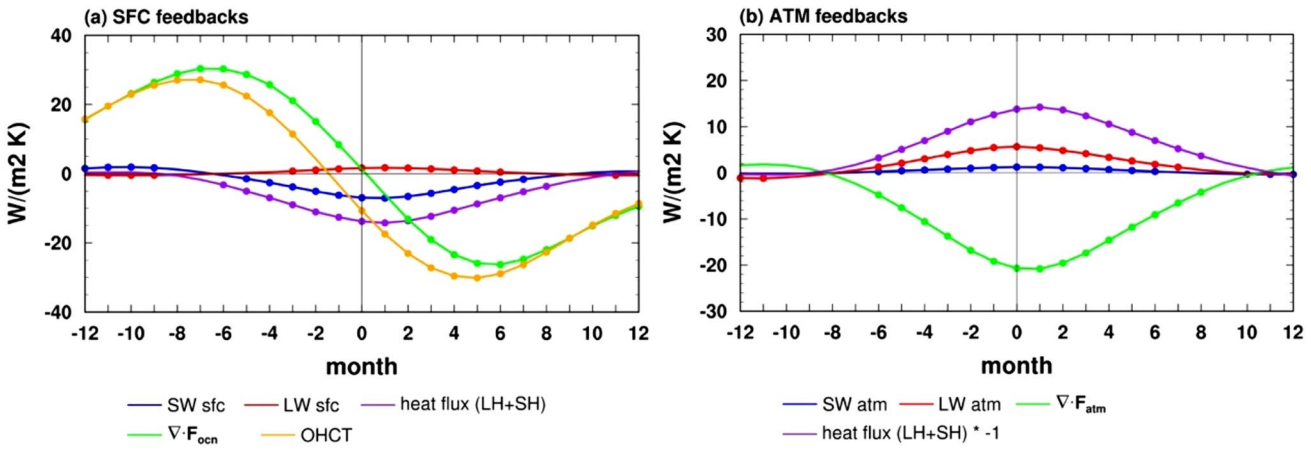

Fig. 5 Lagged feedbacks in the Central Pacific (left) at the surface and (right) in the atmosphere. Negative lags mean that the flux leads ONI index. Dots indicate that the results pass the 95% significance test

the ENSO developing phase (Figs. 3q, 5, comparing zero and negative lags). Because of the strong negative radiative and heat flux feedbacks, the OHCT term is of negative value suggesting a dampening effect on SST warming (Fig. 3r).

3.1.3 Atmosphere

The LW radiative feedbacks in the atmosphere are dominated by the cloud LW feedback, while the SW radiative feedback is most attributed to the concentration of water vapor (Fig. 4). As explained above, the increased SST and air temperature results in a positive and negative radiative feedback in the atmosphere, respectively. There is a remarkable compensation between the radiative and non-radiative feedbacks. The positive radiative feedback by clouds in the Central Pacific is largely offset by the horizontal energy transport feedback. The energy tendency (the overall energy accumulation) in the atmosphere is small, being less than 1 W/(m^2 K), because of the low heat capacity of the atmosphere.

Another compensation exists in the horizontal energy transports in the atmosphere. The major negative feedback in the atmosphere is from the horizontal divergence of the dry static energy which is largely canceled out by the convergence of water vapor. The compensation of the horizontal transport between the dry static energy and water vapor yield a net negative feedback of horizontal energy transport during El Niño (Fig. 4p), which is mainly due to a strengthening of poleward energy transport (not shown). While this results in a small tropical mean horizontal energy transport, the difference of horizontal transport of latent heating between the Warm Pool and Central Pacific leads to a significant differential heating in the atmosphere, which is essential to the change of atmospheric circulation, see Sect. 3.4 for more details.

3.2 Comparison of cloud feedbacks in the kernel and *CRF* methods

The results above show that cloud feedbacks are the most important radiative feedbacks during ENSO. However, previous studies suggested that several factors can lead to uncertainties in the cloud feedback quantification, such as discrepancies between different datasets, the method used to measure the cloud feedback (Sun and Trenberth 1998; Sun et al. 2006; Dessler 2013). Therefore, we use multiple datasets to measure the uncertainties in the cloud feedback. To simplify the expression, we use dR_c and $dCRF$ to

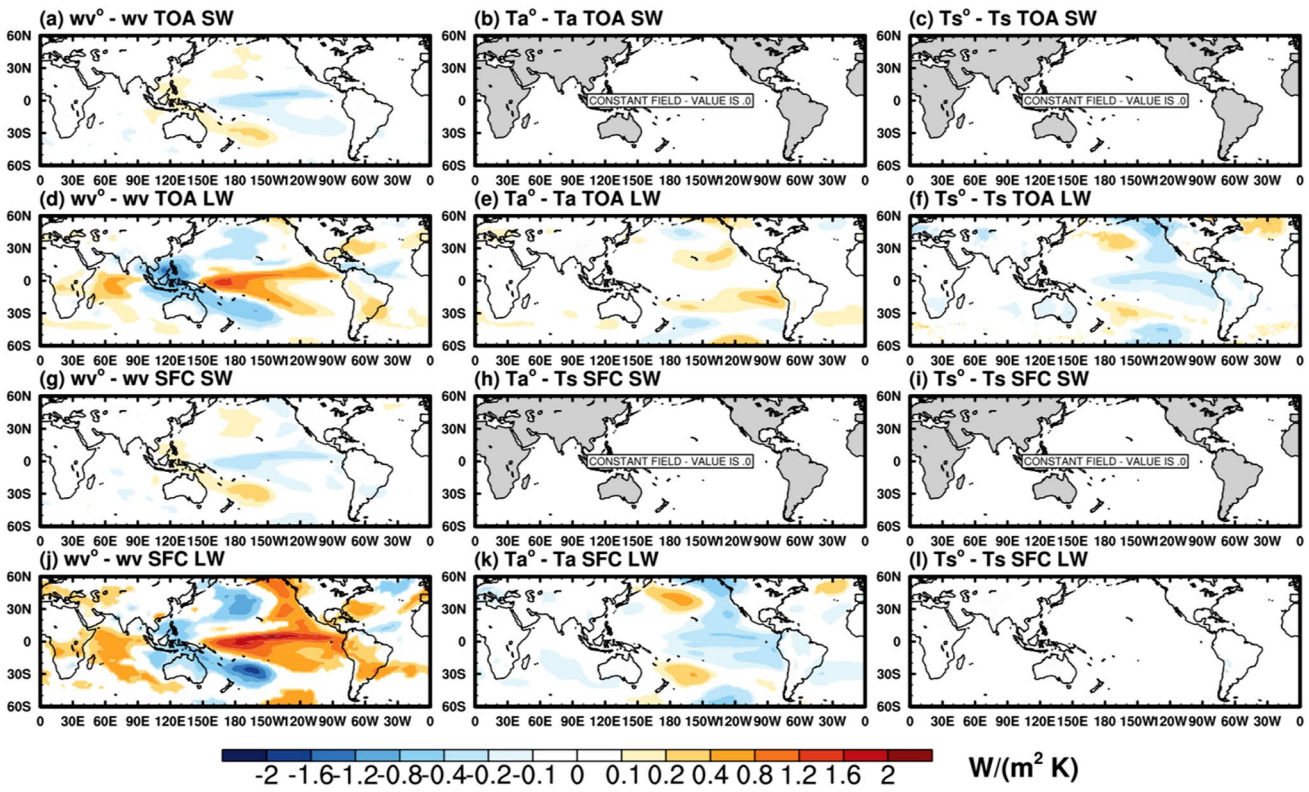

Fig. 6 The difference of non-cloud feedbacks between clear-sky and all-sky. **a**, **b**, **c**, **g**, **h**, **i** SW feedbacks. **d**, **e**, **f**, **j**, **k**, **l** LW feedbacks. *wv* denotes the water vapor feedback; T_a the air temperature feedback; T_S is the surface temperature feedback. Superscript ° denotes feedbacks in clear-sky. Note that only values passing the 95% significance test are contoured in color

represent the cloud feedback measured by the kernel method and by the cloud radiative forcing method respectively in this section.

In terms of the method difference, the main difference of cloud feedback between the kernel method (dR_c) and cloud radiative forcing method ($dCRF$) is from the difference of the non-cloud components between clear-sky and all-sky [as shown in Eq. (5)], which is primarily due to water vapor (Fig. 6). Equation (5) can be rewritten as:

$$dR_c = dCRF + \left(dR^o_{wv} - dR_{wv}\right) \tag{11}$$

The results in Table 1 suggest that compared with dR_c, $dCRF$ tends to underestimate the cloud feedback, e.g. the cloud SW feedbacks both at the TOA and the surface and the cloud LW feedback at the TOA. This is because the difference of the water vapor kernel between clear-sky and all-sky $\left(dR^o_{wv} - dR_{wv}\right)$ due to the damping of water vapor sensitivities by the existence of clouds is of the same sign as $dCRF$. Ignoring this effect would alias water vapor effect as the cloud feedback, which suggests that the kernel method is a more accurate method for quantifying the cloud feedback. The surface LW cloud feedback from both methods is weak because the high concentration of water vapor in the Central Pacific dampens radiation's sensitivity to clouds. dR_c LW and $dCRF$ LW at the surface are of the opposite signs, which is also due to the damping of water vapor sensitivities by the existence of clouds. This discloses the non-negligible impact on the quantification of cloud feedback due to methodological differences.

Clear-sky radiation difference-caused discrepancies between various datasets are also shown in Table 1. The cloud LW feedback from CERES Ed4.0, CERES Ed4.1 C, and CERES Ed4.1 T show some quantitative differences which are induced by the different ways of computing clear-sky radiation among various products. In CERES Ed4.0 and CERES Ed4.1 C, clear sky represents cloud-free regions, while in CERES Ed 4.1 T and most GCM models clear-sky radiation is computed by artificially removing clouds while keeping other fields such as water vapor unchanged in the computation. For the cloud SW feedback, the results show less discrepancy. Together these results show that the uncertainty associated with cloud feedback due to the discrepancies in observational datasets is relatively small and is of less concern than the uncertainty induced by different methods (dR_c vs. $dCRF$).

3.3 Accumulated effects

To investigate how the different energy fluxes drive the evolution of SST, we focus next on the flux changes 6 months ahead of SST change and call them accumulated effects to distinguish them from the feedbacks. The accumulated effects are obtained by summing flux anomalies for the 6 months ahead of SST change and then regressed to the ONI index, e.g. the anomalous accumulated energy flux for December 2015 is the sum of energy flux anomalies from July to December of 2015. This 6 month accumulation period is used because the vertical flux starts to have significant effects around 6 months before the peak of the SST anomaly (Fig. 5). Table 2 lists the 6-month accumulated effect of each flux in the Central Pacific. At the TOA, the SW accumulated effect is primarily due to cloud change and the LW accumulated effect is caused by both cloud and water vapor changes, with the cloud LW accumulated effect being approximately twice as strong as the water vapor accumulated effect. The net positive accumulated radiative effect

Table 1 Cloud feedbacks from CRF method ($dCRF$) and kernel method (dR_c) at the (upper) TOA and (lower) the surface in the Central Pacific

Cloud feedback W/(m^2 K)	dR_c SW TOA	$dCRF$ SW TOA	dR_c LW TOA	$dCRF$ LW TOA
CERES Ed4.0 (all) ERA5 (clr)	− 7.44 ± 1.04	− 7.19 ± 1.01	7.51 ± 0.70	7.17 ± 0.64
CERES Ed4.0 (all and clr)	− 7.10 ± 1.00	-6.84 ± 0.97	8.10 ± 0.74	7.75 ± 0.69
CERES Ed4.1 C (all and clr)	− 7.10 ± 1.00	− 6.84 ± 0.97	8.10 ± 0.74	7.75 ± 0.69
CERES Ed4.1 T (all and clr)	− 7.02 ± 0.99	− 6.78 ± 0.96	7.23 ± 0.69	6.89 ± 0.63
Cloud feedback W/(m^2 K)	dR_c SW SFC	$dCRF$ SW SFC	dR_c LW SFC	$dCRF$ LW SFC
CERES Ed4.0 (all) ERA5 (clr)	− 7.02 ± 1.05	− 6.80 ± 1.03	*− 0.08 ± 0.21*	− 1.14 ± 0.17
CERES Ed4.0 (all and clr)	− 6.93 ± 1.02	− 6.71 ± 1.00	0.54 ± 0.25	− 0.52 ± 0.18
CERES Ed4.1 C (all and clr)	− 6.86 ± 1.02	− 6.64 ± 1.00	0.50 ± 0.24	− 0.56 ± 0.18
CERES Ed4.1 T (all and clr)	− 6.65 ± 1.01	− 6.43 ± 0.99	0.33 ± 0.24	− 0.73 ± 0.18

Italics indicate insignificant results. Error bars represent the 95% confidence interval of each feedback

Table 2 Summary of accumulated effects for 6 months over the Central Pacific

		Regression coefficient W/(m^2 K)			Explained variance R^2		
		TOA	SFC	ATM	TOA	SFC	ATM
SW	Total	− 20.72 ± 4.96	− 25.92 ± 5.76	5.20 ± 0.87	0.27	0.30	0.43
	Cloud	− 22.54 ± 5.04	− 20.77 ± 4.87	− 1.77 ± 0.21	0.30	0.28	0.59
	Water vapor	1.57 ± 0.24	− 6.11 ± 0.86	7.68 ± 1.10	0.47	0.51	0.50
LW	Total	30.36 ± 5.53	5.39 ± 1.75	24.98 ± 4.01	0.39	0.17	0.45
	Cloud	26.73 ± 4.32	1.35 ± 0.59	25.38 ± 3.81	0.45	0.10	0.48
	Water vapor	17.02 ± 2.64	14.19 ± 1.86	2.83 ± 1.14	0.47	0.55	0.12
	$\boldsymbol{T_a}$	− 6.68 ± 1.35	7.30 ± 0.84	− 13.98 ± 2.16	0.34	0.61	0.47
	$\boldsymbol{T_s}$	− 2.55 ± 0.24	− 14.78 ± 1.46	12.23 ± 1.22	0.70	0.68	0.68
Net radiative flux		9.64 ± 1.45	− 20.53 ± 4.17	30.18 ± 4.75	0.48	0.34	0.46
			Ocean	ATM		Ocean	ATM
Latent heat by condensation		–	–	149.13 ± 27.26	–	–	0.39
SFC heat flux		–	− 57.96 ± 9.502	–	–	0.46	–
$\nabla \bullet F$		–	119.53 ± 28.17	− 88.13 ± 11.97	–	0.27	0.53
$\frac{\partial E}{\partial t}$		–	41.04 ± 35.75	3.36 ± 1.06	–	0.03	0.17

SW and LW are the radiative forcing. The components, such as cloud, water vapor, T_{air}, T_{sfc} are from the kernel method. Net radiative flux is the sum of SW and LW radiation. Latent heat by condensation measures the latent heat release by condensation in the atmosphere. Surface heat flux is the sum of the *LH* and the *SH* at the surface. $\nabla \bullet F$ refers to the atmospheric horizontal energy transport or oceanic energy transport [$\nabla \bullet F_{atm}$ in Eq. (1) and $\nabla \bullet F_{ocn}$ term in Eq. (2)]. $\frac{\partial E}{\partial t}$ is the energy tendency term in the atmosphere or in the ocean. R^2 indicates the fraction of variance of SST in the Central Pacific explained by each variable. Error bars represent the 95% confidence interval of each accumulated effect

suggests the energy accumulation for the atmosphere–ocean system occurs during the ENSO developing phase.

In the ocean, the accumulated effect of oceanic energy transport driven by ocean dynamics provides the most energy to the SST warming and is almost twice as strong as the accumulated effect of radiative and heat fluxes. The radiative and heat flux effects at the surface are both of negative sign with the heat flux effect much stronger than that of radiative fluxes, both of which suppress the SST warming. The SW negative effect is primarily caused by clouds while the LW positive effect is induced by the temperature change in the atmosphere (T_a in Table 2). There is a strong compensation between the surface temperature (T_s in Table 2) and water vapor LW accumulated effects. Due to the aforementioned dampening effect of boundary layer water vapor, the cloud accumulated LW effect does not add much to the LW accumulated effect on the surface.

In the atmosphere the LW accumulated effect dominates, primarily due to the cloud LW effect. Both SW and LW radiative fluxes act as a warming effect and are compensated by the negative horizontal energy transport, leaving a small energy residual in the atmosphere. Latent heat release by condensation (*LC*) is a powerful energy source in the atmosphere and as mentioned before, is mainly offset by the horizontal transport of dry static energy. However, the differential heating induced by *LC* in the atmosphere can strengthen the anomalous atmospheric circulation during ENSO and enhance the SST warming.

3.4 Differential heating in the atmosphere

The differential diabatic heating between the Central Pacific and Warm Pool is of great importance to the circulation response and SST warming (Bony et al. 2013; Xia and Huang 2017). Anomalous SST warmings in the Central Pacific result in an anomalous circulation, with more convection, clouds, and precipitation in the Central Pacific and less of them in the Warm Pool region. The increase of condensation and corresponding *LC* induced by the enhancement of the convergence of water vapor in the atmosphere is the biggest energy source for the atmosphere in the Central Pacific. The decrease of condensation in the Warm Pool regions results in a reduction of *LC*. With more heating and ascending motion in the Central Pacific and less heating and more descending motion of air in the Warm Pool region, the differential heating caused by such a process further increases the anomalous circulation, strengthens the westerly anomaly (the Bjerknes feedback), and helps to trap the warm water over the Central Pacific, which increases the SST warming. The atmosphere gains energy also through the convergence of LW radiation primarily caused by the increase of cloud cover. Although the increase of convective cloud cover in the Central Pacific enhances the Bjerknes feedback and increases the SST warming in that region (Rädel et al. 2016; Kolly and Huang 2018), it also blocks more SW and reduces the amount of SW reaching the

surface which makes a negative feedback to the SST warming (Waliser et al. 1994).

To measure the differential heating between the Central Pacific and Warm Pool region, we define the differential heating as (Bony et al. 2013; Xia and Huang 2017):

$$DH = \langle \Delta R_{cp} \rangle - \langle \Delta R_{wp} \rangle \quad (12)$$

Here DH stands for the differential heating, $\langle \ldots \rangle$ represents regional average, and ΔR_{cp} and ΔR_{wp} are flux anomalies in the 5N–5S, 190E–240E and 5N–5S, 120E–150E regions, respectively. Note that the atmosphere can either be a positive feedback to SST warming by enhancing anomalous atmospheric circulation and the Bjerknes feedback, or negative feedback by reflecting more SW back to the space through the increase of cloud cover. To compare each role of the atmosphere, we use flux anomalies induced by latent energy released by condensation and LW anomalies in the atmosphere to obtain the differential heating. The differential heating obtained in this way represents an atmospheric positive feedback and SW anomalies at the surface in the Central Pacific due to cloud cover represents an atmospheric negative feedback. The differential heating of latent heat by condensation, LW anomalies in the atmosphere, and SW anomalies at the surface measured in this way are 37.91 W/(m^2 K), 5.71 W/(m^2 K), and − 6.96 W/(m^2 K), respectively.

Figure 7 compares the correlations of ONI between the differential heating by condensation and LW anomalies in the atmosphere and the SW anomalies in the Central Pacific at the surface. In general, the differential heating of latent heat by condensation shows a stronger relationship with ONI than that of SW anomalies at the surface in the Nino3.4 region (the SST anomaly that defines ONI), suggesting that the positive DH feedbacks have a stronger influence on surface warming than the local SW negative feedback. Figure S5 in the Supplementary Information further compared the negative (local SW) and positive (LC differential heating) atmospheric feedbacks and affirms this conclusion. Hence, in summary, these results support the idea that the overall atmospheric effect is likely to enhance the SST anomalies during ENSO.

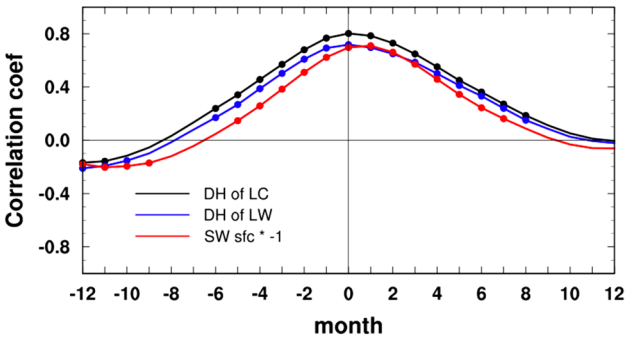

Fig. 7 Lagged correlation coefficient of ONI index and the differential heating (DH) between the Central Pacific (5N–5S, 190E–240E) and Warm Pool (5N–5S, 120E–150E) by latent heat release by condensation (LC) and LW anomalies in the atmosphere, and the SW anomalies at the surface in the Central Pacific. Dots indicate that the results pass the 95% significance test

4 Conclusions

In this paper we compare the roles of energy feedbacks and present a complete picture of how radiative and non-radiative feedbacks evolve during an ENSO cycle. In some aspects, our results are in accord with previous assessments (Waliser et al. 1994; Sun and Trenberth 1998; Kolly and Huang 2018), confirming that the cloud feedbacks contribute the most to the radiative feedback. The net cloud feedback at the TOA is negligible due to the opposite contributions from cloud SW and LW feedbacks, although the cloud SW and LW feedbacks dominate at the surface and in the atmosphere respectively. During the developing phase of El Niño, the horizontal energy transport in the ocean starts to have an effect much earlier than radiative fluxes. Radiative and heat fluxes at the surface begin to suppress the oceanic warming as soon as any significant warming starts, with the strength of the heat flux feedback being stronger than the radiative feedback. To elucidate the overall role of atmospheric feedback—whether it enhances or dampens SST warming, here we compare the relationship between the SST anomaly and the different energetic feedbacks. With the positive feedback of differential heating being more strongly correlated with SST anomalies in the Nino region than the surface SW negative feedback, this supports the idea that the atmospheric feedback is likely an overall positive feedback that acts to strengthen SST warming.

We also assess several factors that can cause the uncertainty of the cloud feedback quantification and find that more discrepancy results from different methods (namely the cloud radiative forcing vs. the kernel methods) of measuring cloud feedbacks than from the use of different datasets. Compared to the results from the cloud radiative forcing method, cloud feedbacks measured by the kernel method is stronger [about 0.3 W/(m^2 K)] in terms of the cloud LW feedbacks at the TOA and the cloud SW feedbacks both at the TOA and the surface. Most notably, because of the difference of radiative sensitivity to water vapor in clear- and cloudy-skies, the sign of cloud LW feedback at the surface from these two methods can be opposite.

In summary, this paper provides a thorough assessment of energy flux feedbacks in ENSO. By combining data from reanalysis and observations, we identify the key

energetic feedbacks and their interactions with respect to TOA, surface and atmospheric budgets, respectively. Different datasets and diagnostic methods are included in this study to measure the uncertainties in the analyzed feedbacks and confirm the robustness of our conclusions. The analysis here suggests that the overall atmospheric effect is likely a positive feedback to ENSO development and this warrants further, experimental confirmation in future studies.

Acknowledgements The ERAI data used in this research can be accessed from https://apps.ecmwf.int/datasets/data/interim-full-moda/levtype=sfc/. The JRA55 dataset can be accessed from https://rda.ucar.edu/datasets/ds628.0/. The ERA5 dataset is from https://cds.climate.copernicus.eu/-!/search?text=ERA5&type=dataset. The CERES data is from https://ceres.larc.nasa.gov/order_data.php. The TRMM data can be accessed from https://disc.gsfc.nasa.gov/datasets/TRMM_3B43_7/summary. The radiative kernel data from Yi Huang's homepage (https://huanggroup.wordpress.com/research/). HH acknowledges a visiting student fellowship provided by China Scholarship Council (CSC) that supported her visit to McGill University where this research is conducted. YH acknowledges a grant from the Natural Sciences and Engineering Research Council of Canada (RGPIN-2019-04511). YYH acknowledges the National Natural Science Foundation of China under grants of 41530423 and 41761144072.

References

Allan RP, Slingo A, Ringer M (2002) Influence of dynamics on the changes in tropical cloud radiative forcing during the 1998 El Niño. J Clim 15:1979–1986

Bayr T, Dommenget D, Martin T, Power SB (2014) The eastward shift of the Walker Circulation in response to global warming and its relationship to ENSO variability. Clim Dyn 43:2747–2763

Bellenger H, Guilyardi É, Leloup J, Lengaigne M, Vialard J (2014) ENSO representation in climate models: from CMIP3 to CMIP5. Clim Dyn 42:1999–2018

Bjerknes J (1966) A possible response of the atmospheric Hadley circulation to equatorial anomalies of ocean temperature. Tellus 18:820–829

Bony S, Bellon G, Klocke D, Sherwood S, Fermepin S, Denvil S (2013) Robust direct effect of carbon dioxide on tropical circulation and regional precipitation. Nat Geosci 6:447–451

Bony S, Dufresne JL (2005) Marine boundary layer clouds at the heart of tropical cloud feedback uncertainties in climate models. Geophys Res Lett. https://doi.org/10.1029/2005GL023851

Cess RD, Zhang M, Wielicki BA, Young DF, Zhou X-L, Nikitenko Y (2001) The influence of the 1998 El Niño upon cloud-radiative forcing over the Pacific warm pool. J Clim 14:2129–2137

Cheng L, Trenberth KE, Fasullo J, Boyer T, Abraham J, Zhu J (2017) Improved estimates of ocean heat content from 1960 to 2015. Sci Adv 3(3):e1601545

Cheng L, Trenberth KE, Fasullo JT, Mayer M, Balmaseda M, Zhu J (2019) Evolution of ocean heat content related to ENSO. J Clim 32:3529–3556

Chiang JC, Sobel AH (2002) Tropical tropospheric temperature variations caused by ENSO and their influence on the remote tropical climate. J Clim 15:2616–2631

Dee DP et al (2011) The ERA-Interim reanalysis: configuration and performance of the data assimilation system. Q J R Meteorol Soc 137:553–597

Dessler A (2013) Observations of climate feedbacks over 2000–10 and comparisons to climate models. J Clim 26:333–342

Dessler AE (2010) A determination of the cloud feedback from climate variations over the past decade. Science 330:1523–1527

Guilyardi E, Braconnot P, Jin F-F, Kim ST, Kolasinski M, Li T, Musat I (2009) Atmosphere feedbacks during ENSO in a coupled GCM with a modified atmospheric convection scheme. J Clim 22:5698–5718

Guilyardi E et al (2004) Representing El Nino in coupled ocean–atmosphere GCMs: the dominant role of the atmospheric component. J Clim 17:4623–4629

Hersbach H et al (2020) The ERA5 global reanalysis. Q J R Meteorol Soc 146:1999–2049

Huang Y, Xia Y, Tan X (2017) On the pattern of CO_2 radiative forcing and poleward energy transport. J Geophys Res Atmos 122:10578–10593

Huffman GJ, Adler RF, Bolvin DT, Nelkin EJ (2010) The TRMM multi-satellite precipitation analysis (TMPA). In: Satellite rainfall applications for surface hydrology. Springer, pp 3–22

Klein SA, Soden BJ, Lau N-C (1999) Remote sea surface temperature variations during ENSO: evidence for a tropical atmospheric bridge. J Clim 12:917–932

Kobayashi S et al (2015) The JRA-55 reanalysis: general specifications and basic characteristics. J Meteorol Soc Jpn Ser II 93:5–48

Kolly A, Huang Y (2018) The radiative feedback during the ENSO cycle: observations versus models. J Geophys Res Atmos 123:9097–9108

Liu Z, Alexander M (2007) Atmospheric bridge, oceanic tunnel, and global climatic teleconnections. Rev Geophy. https://doi.org/10.1029/2005RG000172

Lloyd J, Guilyardi E, Weller H (2011) The role of atmosphere feedbacks during ENSO in the CMIP3 models. Part II: using AMIP runs to understand the heat flux feedback mechanisms. Clim Dyn 37:1271–1292

Lloyd J, Guilyardi E, Weller H (2012) The role of atmosphere feedbacks during ENSO in the CMIP3 models. Part III: the shortwave flux feedback. J Clim 25:4275–4293

Lloyd J, Guilyardi E, Weller H, Slingo J (2009) The role of atmosphere feedbacks during ENSO in the CMIP3 models. Atmos Sci Lett 10:170–176

Loeb NG et al (2018) Clouds and the earth's radiant energy system (CERES) energy balanced and filled (EBAF) top-of-atmosphere (TOA) edition-4.0 data product. J Clim 31:895–918

Mayer M, Haimberger L, Edwards JM, Hyder P (2017) Toward consistent diagnostics of the coupled atmosphere and ocean energy budgets. J Clim 30:9225–9246

Mayer M, Trenberth KE, Haimberger L, Fasullo JT (2013) The response of tropical atmospheric energy budgets to ENSO. J Clim 26:4710–4724

Middlemas EA, Clement AC, Medeiros B, Kirtman B (2019) Cloud radiative feedbacks and El Niño-Southern oscillation. J Clim 32:4661–4680

Pinker R, Grodsky S, Zhang B, Busalacchi A, Chen W (2017) ENSO impact on surface radiative fluxes as observed from space. J Geophys Res Oceans 122:7880–7896

Rädel G, Mauritsen T, Stevens B, Dommenget D, Matei D, Bellomo K, Clement A (2016) Amplification of El Niño by cloud longwave coupling to atmospheric circulation. Nat Geosci 9:106

Radley C, Fueglistaler S, Donner L (2014) Cloud and radiative balance changes in response to ENSO in observations and models. J Clim 27:3100–3113

Roemmich D, Gilson J (2011) The global ocean imprint of ENSO. Geophys Res Lett 38

Sardeshmukh PD, Hoskins BI (1984) Spatial smoothing on the sphere. Mon Weather Rev 112:2524–2529

Shell KM, Kiehl JT, Shields CA (2008) Using the radiative kernel technique to calculate climate feedbacks in NCAR's Community Atmospheric Model. J Clim 21:2269–2282

Soden BJ, Broccoli AJ, Hemler RS (2004) On the use of cloud forcing to estimate cloud feedback. J Clim 17:3661–3665

Stephens GL (2005) Cloud feedbacks in the climate system: a critical review. J Clim 18:237–273

Su H, Jiang JH (2013) Tropical clouds and circulation changes during the 2006/07 and 2009/10 El Niños. J Clim 26:399–413

Sun D-Z (2000) The heat sources and sinks of the 1986–87 El Niño. J Clim 13(20):3533–3550

Sun D-Z, Fasullo J, Zhang T, Roubicek A (2003) On the radiative and dynamical feedbacks over the equatorial Pacific cold tongue. J Clim 16:2425–2432

Sun D-Z, Yu Y, Zhang T (2009) Tropical water vapor and cloud feedbacks in climate models: A further assessment using coupled simulations. J Clim 22:1287–1304

Sun D-Z et al (2006) Radiative and dynamical feedbacks over the equatorial cold tongue: results from nine atmospheric GCMs. J Clim 19:4059–4074

Sun D-Z, Trenberth KE (1998) Coordinated heat removal from the equatorial Pacific during the 1986–87 El Nino. Geophys Res Lett 25:2659–2662

Trenberth KE, Caron JM, Stepaniak DP, Worley S (2002) Evolution of El Niño–Southern Oscillation and global atmospheric surface temperatures. J Geophys Res Atmos 107:AAC 5-1–AAC 5-17

Trenberth KE, Stepaniak DP (2003) Covariability of components of poleward atmospheric energy transports on seasonal and interannual timescales. J Clim 16:3691–3705

Waliser DE, Blanke B, Neelin JD, Gautier C (1994) Shortwave feedbacks and El Niño-Southern Oscillation: forced ocean and coupled ocean–atmosphere experiments. J Geophys Res Oceans 99:25109–25125

Wang H, Su W (2015) The ENSO effects on tropical clouds and top-of-atmosphere cloud radiative effects in CMIP5 models. J Geophys Res Atmos 120:4443–4465

Xia Y, Huang Y (2017) Differential radiative heating drives tropical atmospheric circulation weakening. Geophys Res Lett 44:10592–10600

Zhang T, Sun D-Z (2008) What causes the excessive response of clear-sky greenhouse effect to El Niño warming in community atmosphere models? J Geophys Res Atmos. https://doi.org/10.1029/2007JD009247